Communications in Nonlinear Science and Numerical Simulation 114 (2022) 106604

Contents lists available at ScienceDirect

Communications in Nonlinear Science and Numerical Simulation

journal homepage: www.elsevier.com/locate/cnsns

Short communication

A discussion on nonlocality: From fractional derivative model to peridynamic model

HongGuang Sun [a,b,*], Yuanyuan Wang [a,b], Lin Yu [b], Xiangnan Yu [a,b]

[a] State Key Laboratory of Hydrology-Water Resources and Hydraulic Engineering, Hohai University, Nanjing, Jiangsu 210098, China
[b] College of Mechanics and Materials, Hohai University, Nanjing, Jiangsu 210098, China

ARTICLE INFO

Article history:
Received 11 November 2021
Received in revised form 7 May 2022
Accepted 23 May 2022
Available online 3 June 2022

Keywords:
Fractional derivative model
Peridynamic model
Mean squared displacement
Nonlocality
Super-diffusion

ABSTRACT

Characterization of nonlocality is an open problem in physics and engineering. This paper conducts a detailed investigation on two nonlocal models, namely, the fractional derivative model and the peridynamic model for anomalous diffusion. A generalized nonlocal model combining the advantages of the fractional derivative model and the peridynamic model, is introduced. In this paper, analytical solutions and the mean squared displacements of the two models are provided and discussed. In addition, their intrinsic relations and notable differences are investigated. Preliminary applications indicate that the peridynamic model can well capture an unremarkable transition from normal-diffusion to super-diffusion, while the fractional derivative model presents super-diffusion behaviors in the whole process. At last, a generalized nonlocal operator is proposed as a more general strategy to solve nonlocal problems.

1. Introduction

Nonlocality has been widely documented in nature and engineering fields, including anomalous diffusion [1], material fracture [2] and structural damage [3]. Thus, nonlocal models, which are capable of well describing the nonlocal processes, have attracted extensive attention in last decades. Different from traditional local models, nonlocal models usually refer to the integro-differential expression to characterize the long-range interaction behaviors in natural systems.

In recent decades, various nonlocal models were proposed [4,5]. Among them, the fractional derivative model (FDM) and the peridynamic model (PDM) attracted the most attention. Because of the convolution with the power-law kernel function, the FDM relates all points in the computational domain. Thus, it can accurately describe the globally correlated and history-dependent behaviors [6–9]. After decades of development, the FDM has been widely used in porous media transports, soft matter mechanics and hydrological processes etc. [10–12]. Additionally, compared to the commonly fractional derivative, the fractional Laplacian is a nonlocal operator contains the inner product of the power function [13].

The PDM, firstly proposed by Silling in 2000 [14], is another popular nonlocal model based on integral operator. The PDM has been successfully applied to deal with various static, dynamic and multi-scale problems [15–20]. The PDM highlights the object interactions within a finite radius of domain, which is defined by an adjacent radius δ, and the interactions between the inside and outside of the adjacent domain are separated [14]. Note that when $\delta \to 0$, the points in the computational domain have no nonlocal interactions and the PDM reduces to a local model. Therefore, δ is a critical

* Corresponding author at: State Key Laboratory of Hydrology-Water Resources and Hydraulic Engineering, Hohai University, Nanjing, Jiangsu 210098, China.
E-mail address: shg@hhu.edu.cn (H. Sun).

https://doi.org/10.1016/j.cnsns.2022.106604
1007-5704/

Nomenclature

$u_F\,(x,t)$	solute concentration for FDM
K_γ	effective diffusion coefficient for FDM
$\gamma\ (1<\gamma\le 2)$	space fractional derivative order
K	spreading rate of the dispersion for PDM
$u_P(x,t)$	solute concentration for PDM
H_x	near-field domain of x
x'	adjacent point
$V_{x'}$	volume belongs to x'
$d(x',x)$	micro-diffusivity function
δ	near-field ranges
$F\{u_F(x,t);x\to k\}$	Fourier transform
$F^{-1}\{u_F(k,t);k\to x\}$	Fourier inverse transform
$G\,(x,t)$	Green function
$u_F(k,s)$	Fourier and Laplace transform of $u_F(x,t)$
$\delta(x)$	Dirac function

factor, which determines the nonlocal behavior [21]. Nevertheless, compared to the FDM, the weight function, used to quantify the degree of interaction of the PDM, is specified as a Gaussian kernel, leading to faster decaying tails.

In summary, there are three major differences between the FDM and the PDM. The first difference is the mathematical framework. The FDM adopts convolution operator while the PDM uses integral operator [22,23]. Another difference is the kernel function approximation. The FDM commonly adopts the power function while the PDM employs the Gaussian function in most cases [24,25]. The last difference is the range of nonlocality. The FDM represents a global correlated nonlocality while the PDM restricts the nonlocal area by a finite radius δ. To further explore the advantages and differences of the two nonlocal models, detailed comparisons are highly desired. This paper aims to conduct a detailed investigation on the FDM and the PDM and further propose a generalized non-local model to make full use of their advantages. To better understand the physical characteristics, a typical nonlocal physical process, anomalous diffusion, is taken as an example to investigate the nonlocality expressed by the two models.

The rest of this paper is organized as follows. In Section 2, the governing equations of the two models are presented, of which the analytical solutions and the mean squared displacement (MSD) are obtained by the Fourier–Laplace transform. In Section 3, two practical applications are conducted to demonstrate the applicability of the two models, followed by detailed comparisons and discussions. Some concluding remarks are provided in Section 4.

2. Mathematical models

2.1. Governing equations

The governing equation of the FDM to describe anomalous diffusion is expressed as [26]

$$\frac{\partial u_F\,(x,t)}{\partial t}=K_\gamma\frac{\partial u_F^\gamma\,(x,t)}{\partial x^\gamma},\quad 1<\gamma\le 2, \tag{1}$$

where $u_F\,(x,t)$ is the solute concentration for FDM, x is the location of points, t denotes ordinary time, K_γ denotes the effective diffusion coefficient for FDM and $\gamma\ (1<\gamma\le 2)$ represents the space fractional derivative order. When $\gamma=2$, Eq. (1) reduces to the classical diffusion equation. Based on the definition of the Riesz potential [27], the space fractional operator is defined as

$$\frac{\partial u_F^\gamma\,(x,t)}{\partial x^\gamma}=D^\gamma u_F\,(x,t)=\int_R k_\gamma\left(x-x'\right)u_F\left(x',t\right)dx'. \tag{2}$$

Note that the Riesz fractional potential with the nonlocal power-law kernel was defined by Kilbas et al. [28], and $k_\gamma\left(x-x'\right)=2^\gamma\pi^{1/2}\Gamma\,(2/\gamma)\,\Gamma\,(1-\gamma/2)\left|x-x'\right|^{\gamma-1}$. Here, the FDM involves global interactions in R [29].

For comparison purposes, the governing equation of the PDM for diffusion is given as [7]

$$\frac{\partial u_P(x,t)}{\partial t}=K\int_{H_x}\{\underline{H}[x,t]\langle x',x\rangle-\underline{H}[x',t]\langle x,x'\rangle\}dV_{x'}, \tag{3}$$

where K is the spreading rate of the dispersion for PDM, $u_P(x,t)$ is the solute concentration for PDM. Then, $\underline{H}[x,t]\langle x',x\rangle$ and $\underline{H}[x',t]\langle x,x'\rangle$ are the fluid density. H_x is the near-field domain of x, x' is adjacent point.

2.2. Analytical solutions

For Eq. (1), the Pseudo differential operator with the Fourier symbol is used to represent the spatial fractional derivative [30]. Then its characteristics closely related to the inversion of the Riesz potential are employed to solve the operator

$$\left(F\frac{d^{\gamma}}{d\left|x\right|^{\gamma}}u_F\right)(k)=-\left|k\right|^{\gamma}\hat{u}_F(k),\quad 1<\gamma\leq 2,\ k\in R, \tag{4}$$

where $\hat{u}_F(k)=(Fu_F)(k)=\int_{-\infty}^{+\infty}e^{+ikx}u_F(x)\,dx$ and F represents the Fourier transform. For Eq. (1), the initial condition is $u_F(x,0)=\varphi(x)$, $x\in R$ while the boundary condition is $u_F(\pm\infty,t)=0, t>0$. Here, an explicit formula for Green function of Eq. (1) is introduced and the solution to Eq. (1) is assumed to be

$$u(x,t)=\int_{-\infty}^{+\infty}G(x-\xi,t)\,\varphi(\xi)\,d\xi,\quad x\in R,\quad t>0, \tag{5}$$

where $G(x-\xi,t)$ denotes the Green function [31]. Using the Mellin integral transform and the inverse Mellin integral transform, the following formula can be obtained

$$G(x,t)=\frac{1}{\sqrt{\pi}\gamma\left|x\right|}\frac{1}{2\pi i}\int_{\Upsilon-i\infty}^{\Upsilon+i\infty}\frac{\Gamma\left(\frac{s}{\gamma}\right)\Gamma\left(\frac{1}{2}-\frac{s}{2}\right)}{2^{s}\Gamma\left(\frac{s}{2}\right)}\left(\frac{t^{\frac{1}{\gamma}}}{\left|x\right|}\right)^{-s}ds,\quad 0<\Upsilon<1. \tag{6}$$

For Eq. (6), it is necessary to convert the contour of integration into the loop $L_{+\infty}$ encircling all the poles $s_k=\gamma(1+k)$, $k=0,1,2,\ldots$ and $s_m=2m+1, m=0,1,2,\ldots$ of the functions $\Gamma(1-s/\gamma)$ and $\Gamma(1/2-s/2)$, respectively. Then, Eq. (6) can be rewritten as

$$G(x,t)=\frac{1}{\pi\gamma t^{1/\gamma}}\sum_{k=0}^{\infty}\frac{\Gamma((2k+1)/\gamma)}{(2k)!}\left(-\frac{x^2}{t^{2/\gamma}}\right)^{k},\quad 1<\gamma\leq 2. \tag{7}$$

The solution to Eq. (1) with $1<\gamma\leq 2$ is given by the following formula:

$$\begin{aligned}u_F(x,t)&=\int_{-\infty}^{+\infty}G(x-\xi,t)\,\varphi(\xi)\,d\xi\\&=\int_{-\infty}^{+\infty}\frac{1}{\pi\gamma t^{1/\gamma}}\sum_{k=0}^{\infty}\frac{\Gamma((2k+1)/\gamma)}{(2k)!}\left(-\frac{(x-\xi)^2}{t^{2/\gamma}}\right)^{k}d\xi,\quad x\in\mathbb{R},\ t>0.\end{aligned} \tag{8}$$

Here, only the main idea of the derivation process is summarized. For more details, interested readers are referred to Ref. [32].

For the PDM, to derive an analytical solution to Eq. (3), the formula of the inverse Fourier transform can be considered

$$u_P(x)=\left(F^{-1}\hat{u}_P\right)(x)=\frac{1}{2\pi}\int_{-\infty}^{+\infty}e^{-ikx}\hat{u}_P(k)\,dk,\quad \text{if } \hat{u}_P\in L_1(R). \tag{9}$$

Since the weight function of PDM is a Gaussian function, the Gaussian asymptotic result can be obtained from Eq. (9). Assuming $a=\frac{4}{\delta^2}$, we get

$$\begin{aligned}\hat{u}_P(k,t)&=\exp\left(Kt\sqrt{\frac{\pi}{a}}e^{-\frac{k^2}{4a}}\right)\\&=1+Kt\sqrt{\frac{\pi}{a}}e^{-\frac{k^2}{4a}}+\frac{1}{2}\left(Kt\sqrt{\frac{\pi}{a}}e^{-\frac{k^2}{4a}}\right)^{2}+\frac{1}{6}\left(Kt\sqrt{\frac{\pi}{a}}e^{-\frac{k^2}{4a}}\right)^{3}+\cdots+\frac{1}{n!}\left(Kt\sqrt{\frac{\pi}{a}}e^{-\frac{k^2}{4a}}\right)^{n}.\end{aligned} \tag{10}$$

As k approaches infinity, $\hat{u}_P(k,t)$ is increasingly close to 1. In other words, Eq. (10) is convergent. Then the following solution by the inverse Fourier transform is obtained

$$u_P(x,t)=\delta(x)+Kt2\pi e^{-4a\pi^2x^2}+\frac{1}{2}K^2t^2\sqrt{\frac{\pi}{a}}\sqrt{2}\pi e^{-2a\pi^2x^2}+\cdots+\frac{1}{n!}K^nt^n\left(\sqrt{\frac{\pi}{a}}\right)^{n-1}\sqrt{\frac{4}{n}}\pi e^{-\frac{4}{n}a\pi^2x^2}. \tag{11}$$

Thus, the analytical solution of the PDM diffusion equation with the Gaussian kernel function is given as the series expression

$$u_P(x,t)=\delta(x)+\sum_{k=1}^{\infty}\frac{1}{k!}K^kt^k\left(\delta\sqrt{\pi}\right)^{k-1}\sqrt{k\pi}\,e^{-\frac{16}{k\delta^2}\pi^2x^2}, \tag{12}$$

where $\delta(x)$ denotes the Dirac function. In Eq. (12), $u_P(x,t)$ converges to $\delta(x)$, when k approaches infinity.

2.3. MSD expressions of the two models

In the scheme of the FDM, the infinite waiting time results in a non-Markovian process while the jump length with infinite variance leads to a non-Gaussian propagation. For a broad range of systems, the MSD is usually modeled with a Poisson distribution for the waiting time and a Lévy distribution for the jump length, respectively. Thus, the MSD can be used to characterize the nonlocal diffusion phenomenon, i.e., [33]

$$\varphi(k) = \exp(-\sigma^{\gamma}|k|^{\gamma}) \sim 1 - \sigma^{\gamma}|k|^{\gamma}, \quad 1 < \gamma < 2. \tag{13}$$

Here, to illustrate the explicit dependence on the related variables, the expression of the Laplace transform and Fourier transform is given as

$$u_F(k,s) = F\{L\{u_F(x,t); t \to s\}; x \to k\}, \tag{14}$$

where $u_F(k, s)$ represents the Fourier transform and Laplace transform of $u_F(x, t)$.

With the Fourier and Laplace inversion, the governing equation for FDM can be transformed as

$$\frac{\partial u_F(x,t)}{\partial t} = K_{\gamma\,-\infty}D_x^{\gamma}u_F(x,t). \tag{15}$$

In one dimension, the Weyl operator ${}_{-\infty}D_x^{\gamma}$ equals to the fractional Riesz operator [34], and the Fourier transform of $u_F(x, t)$ is

$$u_F(k,t) = \exp\left(-K_{\gamma}t|k|^{\gamma}\right), \quad 1 < \gamma \le 2. \tag{16}$$

This is a closed-form representation of a Lévy stable expression. When $\gamma \to 2$, the classical Gaussian solution is recovered by the standard theorem of the Fox functions. A power-law asymptotic result can be achieved

$$u_F(x,t) \sim \frac{K_{\gamma}t}{|x|^{1+\gamma}}, \quad 1 < \gamma < 2. \tag{17}$$

The MSD can be computed with the Fox function. Now the definition of $\Delta t = (L_1 - L_2)t^{1/\gamma}$ is introduced. By using the Lévy distribution, the MSD of the space fractional derivative equation is

$$\left\langle x^2(t)\right\rangle \sim \int_{L_1 t^{1/\gamma}}^{L_2 t^{1/\gamma}} dx x^2 u_F(x,t) \sim t^{2/\gamma}. \tag{18}$$

For the PDM, $g(x', t) = e^{-\alpha x'}$ is defined and the following operator is used

$$F\left(\int_{-\infty}^{\infty}\left(g\left(x-x',t\right)\right)\left(f\left(x',t\right)\right)dx'\right) = \hat{g}(k,t)\hat{f}(k,t), \tag{19}$$

where $\hat{g}(k, t)$ denotes the Fourier transform of $g(x, t)$ and $\hat{f}(k, t)$ is the Fourier transform of $f(x', t)$. For $\hat{g}(k, t)$,

$$\hat{g}(k,t) = \int_{-\infty}^{\infty} e^{-ax^2 - jkx}dx, \tag{20}$$

where j is a unit imaginary number. Assuming $u = \sqrt{a}x + jk/2\sqrt{a}$ and Eq. (21) can be further expressed as

$$\hat{g}(k,t) = \sqrt{\frac{\pi}{a}}e^{-\frac{k^2}{4a}}. \tag{21}$$

Fourier transform of Eq. (3) is conducted and Eq. (22) is substituted into Eq. (3). Then the following form is obtained

$$\frac{d\hat{u}_P(k,t)}{dt} = K\sqrt{\frac{\pi}{a}}e^{-\frac{k^2}{4a}}u_P(k,t). \tag{22}$$

Next, using initial point source condition $\hat{u}_P(k, 0) \equiv 1$, we obtain

$$\hat{u}_P(k,t) = \exp\left(Kt\sqrt{\frac{\pi}{a}}e^{-\frac{k^2}{4a}}\right). \tag{23}$$

For the PDM with the Gaussian kernel function, the natural boundary condition is $\lim_{x\to\infty}u_P(x,t) = 0$ and an initial condition is $u_P(x, 0) = \delta(x)$. The MSD can be derived by the formula $\left\langle x^2(t)\right\rangle = -\lim_{k\to 0}\left(\frac{\partial^2}{\partial k^2}\right)\hat{u}_P(k,t)$. Here k is the Fourier transform parameter, and $\hat{u}_P(k,t)$ represents the Fourier transform of $u_P(x,t)$. Therefore, using Eq. (10), the limit form of the MSD can be expressed as

$$\left\langle x^2(t)\right\rangle = Kt\frac{\delta\sqrt{\pi}}{2}\left(\frac{\delta^3}{16}\right)\exp\left(ct\frac{\delta\sqrt{\pi}}{2}\right). \tag{24}$$

Table 1
Parameters in the analytical solution of the PDM.

Spatial unit (dx, mm)	Near-field range (δ, mm)	m-convergence
3.33	10	3
3.33	20	6
3.33	30	9

3. Discussions

3.1. Model comparisons: Nonlocality and kernel functions

As a nonlocal model, the FDM has been widely used to describe the temporal memory and long-range correlations of physical behaviors. Due to the differential–integral operator, the FDM can accurately characterize different power-law tails [35]. In contrast, the PDM mainly used in the field of solid mechanics, based on the nonlocal theory of continuous media [36]. The PDM employs displacement rather than displacement derivative in its formulation. Thus, the PDM usually restates the motion equation in solid mechanics to better describe fracture and crack propagation processes [37].

Although both the FDM and the PDM are nonlocal models, their nonlocality mechanisms and expressions are different. Their nonlocality discrepancies can be investigated from two aspects. The first one is the mathematical and physical origin. Based on convolution operators, the FDM is a powerful mathematical tool in modeling transport processes with strong memory. For the time fractional derivative equation, the integral term reflects the history-dependence of the system function while the spatial fractional derivative equation can accurately describe the path dependence of the mechanical behaviors in complex fractal structures. Different from the FDM with convolution operators, the PDM adopts integral operators. Thus, the state of each point in the PDM relates to the points located in its vicinity. The near-field range of the PDM can be adjusted to the space–time scale of the problem, which enables the PDM to carry out multi-scale analysis under a unified computational framework.

The other aspect is the kernel function. The kernel function of the FDM is a typical nonlocal kernel function with power law characteristics. Hence, the power-law kernel function of the FDM plays a key role in describing the nonlocality of anomalous diffusion. Meanwhile, the PDM uses Gaussian function as the kernel function in most cases. The Gaussian kernel function highlights the interactions among adjacent points while it weakens the interactions among the points outside the adjacent domain. Thus, its influence on the nonlocality intensity and the convergence speed is limited. In other words, Gaussian kernel function weakens the degree of nonlocality of the PDM.

3.2. Model comparisons: MSD of diffusion processes

MSD is an important statistical expression to characterize diffusion processes [38]. Many properties of anomalous diffusion, such as the super- and the sub-diffusion behaviors, can be explored from the analysis of MSD. In this section, the FDM and the PDM are compared by exploring their MSD curves. It is worth noting that there is no clear expression of the MSD for the two models, apart from some simple cases. Here the MSD tests are performed to investigate the nonlocality diversity between two models. In this study, the nonlocality of the PDM is investigated by the m-convergence test. The m-convergence is defined as the ratio of the near-field range to the spatial unit, i.e., $m=\delta/dx$. Detailed values of the spatial unit, near-field range and spatial step size are given in Table 1. The length L is taken to be 1 m.

It can be seen from Fig. 1 that when m takes different values, the initial MSD of the PDM is consistent with that of the classical model. At a later stage, the PDM shows weak super-diffusion features. As m decreases, the super-diffusion features of the PDM gradually disappear. In contrast, the MSD profiles of the FDM show clear super-diffusion behaviors. It seems that the FDM can better characterize super-diffusion features than the PDM, based on the comparison of MSD curves.

3.3. Model comparisons: Concentration profiles and experimental data analysis

In the worked examples, an instantaneous source is placed in the center of the space domain. The diffusion coefficient K_γ is taken to be 1 cm^γ s^{-1}. In Fig. 2, Non-Gaussian phenomena are observed from the analytical results of the FDM, due to the memory form characterized by the power-law kernel function. In the super-diffusion, the heavy-tail phenomenon is stronger with a decrease in the fractional derivative and the peak value decreases dramatically. It indicates that the FDM can characterize nonlocality of anomalous diffusion and the smaller the index γ is, the stronger the super-diffusion behavior is. In contrast to the FDM, the heavy-tailing phenomena are not observed in the analytical results of the PDM. Besides, the m-convergence test reveals that the peak of the PDM decreases with the increase of the nonlocal ratio m. It indicates that the PDM with larger m values can better describe the nonlocal characteristics of diffusion processes. However, due to the use of Gaussian kernel function, the analytical results of the PDM do not show obvious heavy-tailing phenomena.

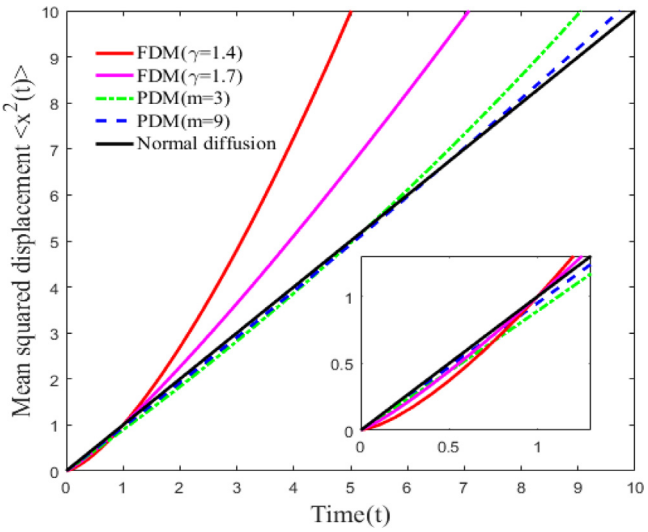

Fig. 1. MSD curves captured by the FDM and the PDM under an instantaneous source, with diffusion coefficients $K = 1$ cm^2 s^{-1} and $K_\gamma = 1$ cm$^\gamma$ s^{-1}.

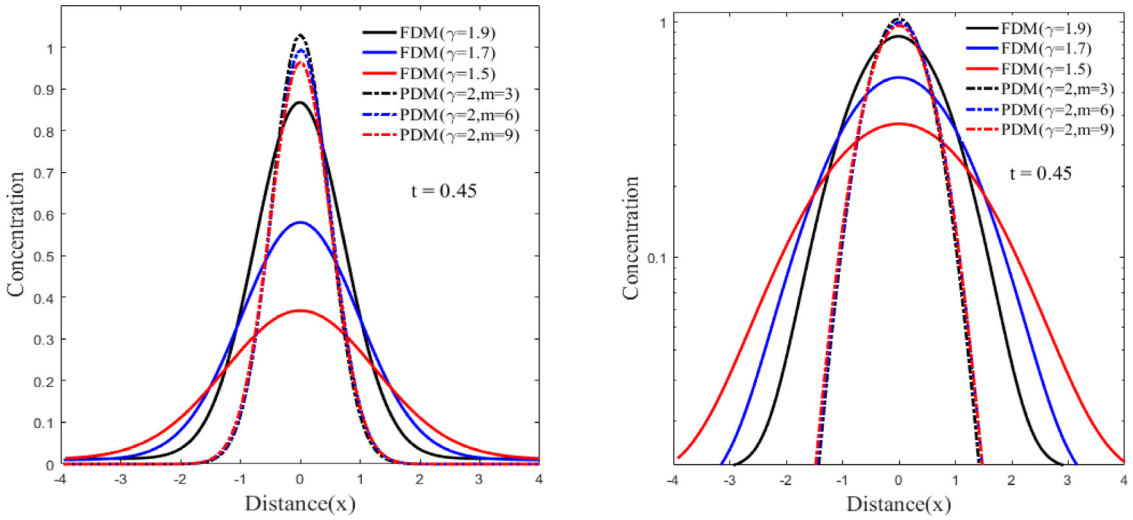

Fig. 2. Concentration profiles of the FDM for different γ values ($\gamma = 1.5$, 1.7 and 1.9) and the PDM for different m values ($m = 3$, 6 and 9) with $\gamma = 2$. The plot on the right side is the semi-log form.

Here an average error is defined as

$$Average\ Error = \frac{1}{n}\sum_{i=1}^{n} |I_{exact}\ (i) - I_{\text{data}}\ (i)| \tag{25}$$

Many studies showed that super-diffusion widely exists in nature and engineering fields, such as biophysics [39], optics [40] and image processing [41]. To further evaluate the performance of the FDM and the PDM, two sets of experimental data from Refs. [42,43] are employed. In Ref. [42], the movement of nanoparticles (NPs) in the polyethylene oxide (PEO) solution containing diffused polystyrene nanoparticles is measured. Densely packed PEO molecules slow down the movement of NPs and an increase in the polymer concentration enhances this limiting effect. However, when the concentration of NPs increases and the particle size reaches 40 nm, the MSD has a sign of super-diffusion in a short time. In the beginning, the MSD of NPs is larger than 0, which closely relates to the solute environment and the pore permeability. In Fig. 3(a), the experimental data of NPs can be well simulated by the FDM with a fractional index γ of 1.8. Fig. 4(a) shows that $\gamma = 1.8$ is the best spatial index of the FDM. On the contrary, the PDM cannot well fit the experimental data, though the optimum fitting result for $m = 6$ is used (here the relative error is the smallest one

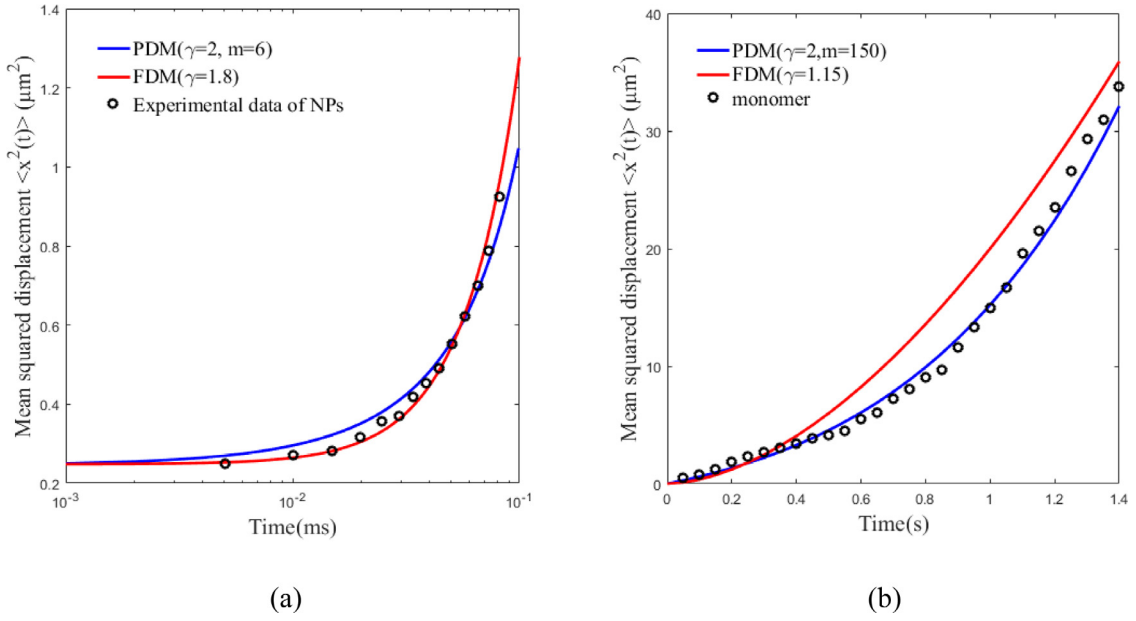

Fig. 3. Comparison of the MSD curves from the experimental data, the FDM and the PDM. The plot (a) is the MSD of NPs (black dots) with a size of 40 nm [41]. The MSD are fitted by the FDM (the red line) with $K_\gamma = 1\mu\text{m}^\gamma\text{s}^{-1}$ and $\gamma = 1.8$, and the PDM (blue line) with parameters $K = 1\ \mu\text{m}^2\ \text{s}^{-1}$, $\gamma = 2$ and $m = 6$. The plot (b) is the MSD of monomers with $K = 2\ \mu\text{m}^2\ \text{s}^{-1}$ [42]. The MSD are fitted by the PDM (blue line) with parameters $K = 2\ \mu\text{m}^2\ \text{s}^{-1}$, $\gamma = 2$ and $m = 150$, and the PDM (red line) with parameters $K_\gamma = 2\ \mu\text{m}^\gamma\ \text{s}^{-1}$ and $\gamma = 1.1$.

compared with other m values in Fig. 5(a)). Here, an increase in the near-field range does not improve the accuracy in describing the super-diffusion phenomenon.

For comparison purposes, a second group of experiment data from Ref. [43] is also provided. In these experiment data, the movement of the membrane-targeting C2A domain of synaptic marker protein 7^{41} (labeled with Atto-565) on a supporting lipid bilayer composed of phosphatidylcholine (PC) and phosphatidylserine (PS) with a ratio of 3:1 is tracked [42]. Based on the above description, the experimental data provide a good example for validating the anomalous diffusion predictions from the FDM and the PDM. It is found that there is a good agreement between the ensemble-averaged MSD of C2A monomers in Fig. 3(b) and that from the PDM with parameters $\gamma = 2$ and $m = 150$. Fig. 5(b) indicates that the near-field range $m = 150$ is the optimum parameter. At the same time, the FDM cannot accurately describe the super-diffusion process with the best spatial index $\gamma = 1.1$ (the best spatial index is shown in Fig. 4(b)). Compared with the strong super-diffusion behavior of the FDM from the initial moment, the PDM can more accurately capture the transition of C2A monomers from normal diffusion to super-diffusion.

3.4. A universal operator based on FDM and PDM

It is clear that the FDM can accurately describe the anomalous diffusion, while the PDM captures the transition from normal diffusion to super-diffusion. Hereby, to combine the advantages of the FDM and the PDM, a generalized nonlocal model is proposed to describe the complex transport processes in natural systems as

$$L_\delta u_\gamma(x) = \int_{R^d} \left[u_\gamma(x) - u_\gamma(y)\right] \gamma_\delta(x,y)dy, \quad 1 < \gamma \le 2, x \in \mathbb{R}^d, \tag{26}$$

where δ is a parameter to measure the scale of nonlocal effect and $\gamma_\delta(x, y)$ is the kernel function, defined as $\gamma_\delta(x, y) = (|x-y|)^{-\gamma}$. It includes the classical diffusion model, the PDM and the FDM as

$$\delta = 1, \quad \gamma = 2 \quad \Rightarrow \quad \lim_{\delta \to 0^+} L_\delta u_\gamma(x) = -\Delta u(x); \tag{27}$$

$$\delta = O(1), \quad \gamma = 2 \quad \Rightarrow \quad \text{PDM}; \tag{28}$$

$$\delta \to \infty, \quad 1 < \gamma \le 2 \quad \Rightarrow \quad \lim_{\delta \to \infty} L_\delta u_\gamma = (-\Delta)^\gamma u. \tag{29}$$

The advantages of the generalized nonlocal model (27) are summarized as follows:

(1) By introducing the power kernel function into the PDM, the PDM can be extended to describe anomalous diffusion with different levels of nonlocality.

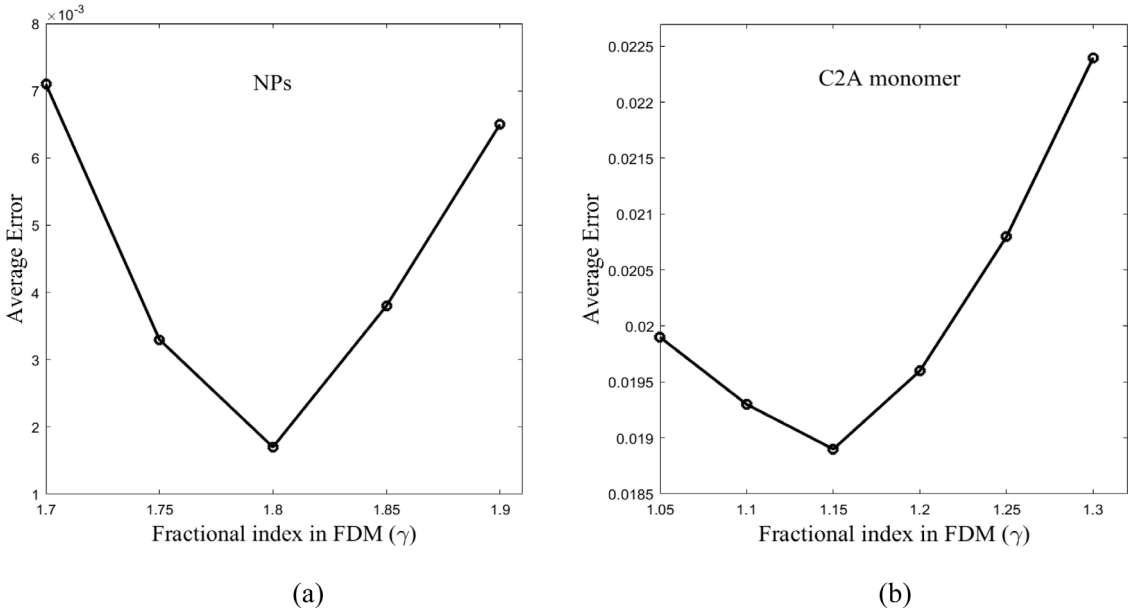

Fig. 4. Error analysis of the experimental data and the analytical results by the FDM (Left corresponds to the fitted results in Fig. 3(a), right side corresponds to the fitted results in Fig. 3(b)).

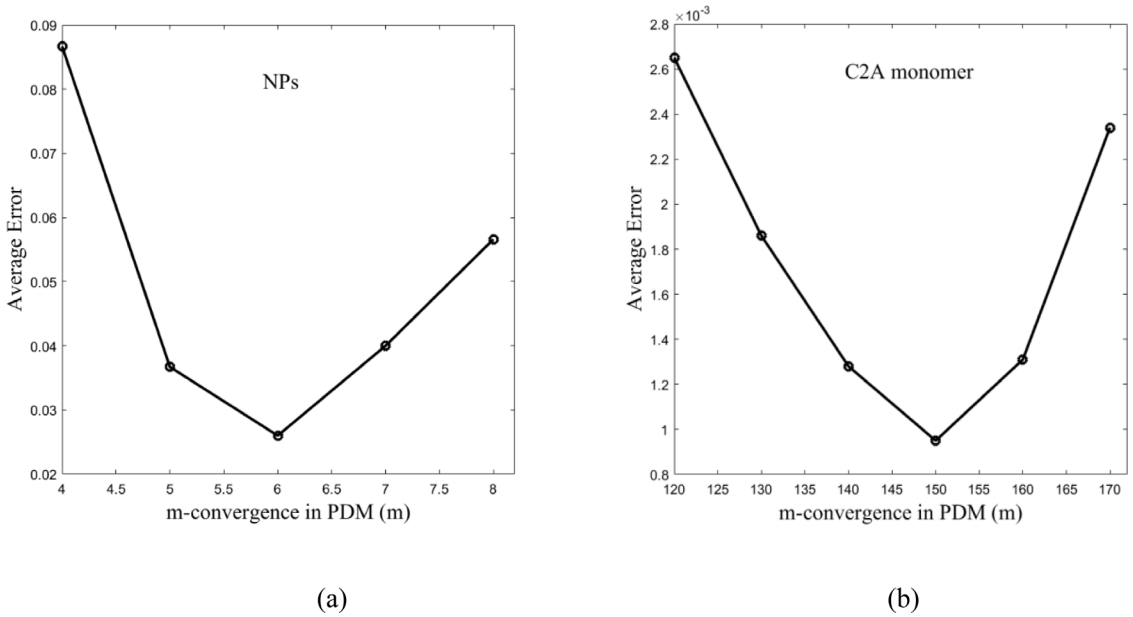

Fig. 5. Error analysis of the experimental data and the analytical results by the PDM (Left corresponds to the fitted results in Fig. 3(a), right side corresponds to the fitted results in Fig. 3(b)).

(2) With a combination of the PDM and FDM, the generalized nonlocal model (27) connects local models and nonlocal models by changing the fractional index and the near-field range.

(3) Madenci et al. [44] proposed a meshless numerical method by using the peridynamic theory, which is capable of solving the nonlocal PDM efficiently. However, the application of the FDM is hindered by the high computational cost of numerical simulations. Hereby, the generalized model can conveniently solve the fractional derivative equation with the help of the fractional Taylor expansion.

4. Conclusions

This paper provides an investigation on two nonlocal mathematical and physical models, namely, FDM and PDM, in characterizing anomalous diffusion to offer a guidance for model selection and further proposes a generalized nonlocal model. Through the analysis of the MSD, analytical experiments and two field applications, it is found that the integral model and the kernel function are the two key factors of the two nonlocal models. Specifically, the power-law kernel function of the FDM can better preserve the nonlocality while the Gaussian kernel function of the PDM limits the nonlocality. Based on the MSD profiles, it is observed that the FDM exhibits obvious super-diffusion features while the PDM can only describe weak super-diffusion behaviors. Two groups of experimental data are also used to test their applicability in characterizing anomalous diffusion. At last, a generalized nonlocal model, which is capable of not only enhancing the ability in describing the nonlocality by using the PDM but also improving the computational efficiency of the FDM, is proposed.

CRediT authorship contribution statement

HongGuang Sun: Conceptualization, Formal analysis, Resources, Writing – review & editing, Funding acquisition. **Yuanyuan Wang:** Conceptualization, Methodology, Software, Validation, Formal analysis, Writing – original draft. **Lin Yu:** Software, Writing – review & editing. **Xiangnan Yu:** Validation, Writing – review & editing.

Declaration of competing interest

The authors declare that they have no known competing financial interests or personal relationships that could have appeared to influence the work reported in this paper.

Acknowledgments

We thank Prof. Ugo Galvanetto (University of Padua) for valuable discussion. This work is supported by the National Natural Science Foundation of China (Nos. 11972148, 41877191), the Natural Science Foundation of Jiangsu Province (No. BK20190024). All authors have read and agreed to the published version of the manuscript.

Appendix

The governing equation of the PDM is given as

$$\frac{\partial u_P(x,t)}{\partial t} = K\int_{H_x}\{\underline{H}[x,t]\langle x'-x\rangle - \underline{H}[x',t]\langle x-x'\rangle\}dV_{x'}, \tag{30}$$

Assume that the fluid density relates only to the absolute difference of the two material points, x and x'

$$\underline{H}[x,t]\langle x'-x\rangle = -\underline{H}[x',t]\langle x-x'\rangle, \tag{31}$$

which leads to the specialized bond-based PD diffusion. In the particular case, the fluid density is defined as

$$\underline{H}[x,t]\langle x'-x\rangle - \underline{H}[x',t]\langle x-x'\rangle = 2\underline{H}[x',t]\langle x-x'\rangle = \underline{H}[x',t]\langle x-x'\rangle \tag{32}$$

So that the PD heat conduction equation can be written as

$$\frac{\partial u_P(x,t)}{\partial t} = K\int_{H_x}\{2\underline{H}[x',t]\langle x-x'\rangle\}dV_{x'} \tag{33}$$

The fluid density function governs the interaction between x and x'. In the case of bond-based PD diffusion, the pairwise interactions are independent of each other, and the fluid between a pair of material points are independent of the concentration difference between other pairs of material points.

For the PD with a single variable [45], the fluid density is defined as

$$\underline{H}[x,t]\langle x'-x\rangle = \frac{1}{2}d(x'-x,t)u_P(x',t) \tag{34}$$

where $u_P(x,t)$ is the solute concentration for PDM, and $d(x'-x,t)$ is the influence function which may have different expressions for different near-field ranges. The Gaussian function $\exp[-\frac{4}{\delta^2}|x-x'|^2]\delta$ (is the near-field range) is widely used as the influence function.

References

[1] Du Q, Gunzburger M, Lehoucq R. Analysis and approximation of nonlocal diffusion problems with volume constraints. SIAM Rev 2012;56:676–96.
[2] Ni T, Pesavento F, Zaccariotto M, Galvanetto U, Schrefler BA. Numerical simulation of forerunning fracture in saturated porous solids with hybrid fem/peridynamic model. Comput Geotech 2021;133:104024.
[3] Shafiei A. Dynamic crack propagation in plates weakened by inclined cracks: an investigation based on peridynamics. Front Struct Civ Eng 2018;12:527–35.
[4] Ren H, Zhuang X, Trung NT, Rabczuk T. Nonlocal operator method for the Cahn-Hilliard phase field model. Commun Nonlinear Sci Numer Simul 2020;96:105687.
[5] Kan XY, Yan JL, Li SF, Zhang AM. On differences and comparisons of peridynamic differential operators and nonlocal differential operators. Comput Mech 2021;68(6):1349–67.
[6] Sun HG, Li ZP, Zhang Y, Chen W. Fractional and fractal derivative models for transient anomalous diffusion: Model comparison. Chaos Solitons Fractals 2017;102:346–53.
[7] Wang YY, Sun HG, Fan SY, Gu Y, Yu XN. A nonlocal fractional peridynamic diffusion model. Fractal Fract 2021;5:76.
[8] Teka WW, Upadhyay RK, Mondal A. Spiking and bursting patterns of fractional-order Izhikevich model. Commun Nonlinear Sci Numer Simul 2018;56:161–76.
[9] Tarasov VE. Fractional dynamics with non-local scaling. Commun Nonlinear Sci Numer Simul 2021;102:105947.
[10] Feng L, Turner I, Perré P, Burrage K. An investigation of nonlinear time-fractional anomalous diffusion models for simulating transport processes in heterogeneous binary media. Commun Nonlinear Sci Numer Simul 2020;92:105454.
[11] Liu YQ, Yin XL, Feng LB, Sun HG. Finite difference scheme for simulating a generalized two-dimensional multi-term time fractional non-Newtonian fluid model. Adv Difference Equ 2018;2018:442.
[12] Alderremy AA, Saad KM, Agarwal P, Aly S, Jain S. Certain new models of the multi space-fractional Gardner equation. Physica A 2020;545:123806.
[13] Li CK, Li CP, Humphries T, Plowman H. Remarks on the generalized fractional Laplacian operator. Mathematics 2019;7(4):320.
[14] Silling S, Zimmermann M, Abeyaratne R. Deformation of a peridynamic bar. J Elasticity 2003;73:173–90.
[15] Soheil B, Farshid M, Arman S. An adaptive thermo-mechanical peridynamic model for fracture analysis in ceramics. Eng Fract Mech 2019;223:106708.
[16] Wang L, Xu J, Wang J. Elastodynamics of linearized isotropic state-based peridynamic media. J Elasticity 2019;137:157–76.
[17] Zaccariotto M, Luongo F, Sarego G, Galvanetto U. Examples of applications of the peridynamic theory to the solution of static equilibrium problems. Aeronaut J 2015;119(1216):677–700.
[18] Buryachenko VA. Variational principles and generalized Hill's bounds in micromechanics of linear peridynamic random structure composites. Math Mech Solids 2020;25(3):682–704.
[19] Li H, Zhang HW, Zheng YG, Ye HF, Lu MK. An implicit coupling finite element and peridynamic method for dynamic problems of solid mechanics with crack propagation. Int J Appl Mech 2018;10(04):1850037.
[20] Guo L, Zhang XY, Li WJ, Zhou X. Multi-scale peridynamic formulations for chloride diffusion in concrete. Eng Anal Bound Elem 2020;120:107–17.
[21] Katiyar A, Foster JT, Ouchi H, Sharma MM. A peridynamic formulation of pressure driven convective fluid transport in porous media. J Comput Phys 2014;261:209–29.
[22] Alotta G, Paola MDi, Pinnola FP. An unified formulation of strong non-local elasticity with fractional order calculus. Meccanica 2021;227.
[23] Romano G, Barretta R. Stress-driven versus strain-driven nonlocal integral model for elastic nano-beams. Composites B 2017;114:184–8.
[24] Chen Z, Bobaru F. Selecting the kernel in a peridynamic formulation: a study for transient heat diffusion. Comput Phys Comm 2015;197:51–60.
[25] Xu X, D'Elia M, Foster JT. A machine-learning framework for peridynamic material models with physical constraints. Comput Methods Appl Mech Engrg 2021;386:114062.
[26] Agwai AG. A peridynamic approach for couple fields [Dissertation], The University of Arizona; 2011.
[27] Samko SG, Kilbas AA, Marichev OI. Fractional integrals and derivatives: Theory and applications. New York and London: Gordon and Breach Science Publishers; 1993.
[28] Kilbas AA, Srivastava HM, Trujillo JJ. Theory and applications of fractional differential equations. North-Holland; 2006.
[29] Macias-Diaz JE. An explicit dissipation-preserving method for Riesz space-fractional nonlinear wave equations in multiple dimensions. Commun Nonlinear Sci Numer Simul 2018;59:67–87.
[30] Saichev A, Zaslavsky G. Fractional kinetic equations: solutions and applications. Chaos 1997;7(4):753–64.
[31] Wright EM. The asymptotic expansion of the generalized hypergeometric function. J London Math 1940;10(1935):287–93.
[32] Gorenflo R, Iskenderov A, Luchko Y. Mapping between solutions of fractional diffusion-wave equations. Fract Calc Appl Anal 2000;3(1):75–86.
[33] Metzler R, Klafter J. The random walk's guide to anomalous diffusion: a fractional dynamics approach. Phys Rep 2000;339(1):1–7.
[34] Jespersen S, Metzler R, Fogedby HC. Lévy flights in external force fields: Langevin and fractional Fokker–Planck equations and their solutions. Phys Rev E 1999;59(3):2736–45.
[35] Zhang Y, Meerschaert MM, Baeumer B. Particle tracking for time-fractional diffusion. Phys Rev E 2008;78(3):036705.
[36] Dayal K, Bhattacharya K. Kinetics of phase transformations in the peridynamic formulation of continuum mechanics. J Mech Phys Solids 2006;54(9):1811–42.
[37] Bie YH, Liu ZM, Yang H, Cui XY. Abaqus implementation of dual peridynamics for brittle fracture. Comput Methods Appl Mech Engrg 2020;372:113398.
[38] Sun HG, Wen C, Hu S, Chen YQ. On mean square displacement behaviors of anomalous diffusions with variable and random orders. Phys Lett A 2010;374(7):906–10.
[39] Peterson VK, Corr CS, Boswell RW, Izaola Z, Kearley GJ. Superfast proton diffusion achieved in a plasma-polymerized fuel-cell membrane. J Phys Chem C 2013;117(9):4351–7.
[40] Hiramoto-Yamaki N, Tanaka K, Suzuki K, Hirosawa KM, Miyahara M, Kalay Z. Ultrafast diffusion of a fluorescent cholesterol analog in compartmentalized plasma membranes. Traffic 2014;15(6):583–612.
[41] Zhu T, Snaider JM, Yuan L, Huang L. Ultrafast dynamic microscopy of carrier and exciton transport. Ann Rev Phys Chem 2019;70:219–44.
[42] Yoshida H, Kaiser V, Rotenberg B, Bocquet L. Supplementary information: Dripplons as localized and superfast ripples of water confined between graphene sheets. Nature Commun 2018;9(1):1496.
[43] Screen HRC, Seto J, Krauss S, Boesecke P, Gupta HS. Extrafibrillar diffusion and intrafibrillar swelling at the nanoscale are associated with stress relaxation in the soft collagenous matrix tissue of tendons. Soft Matter 2011;7(23):11243.
[44] Madenci E, Barut A, Dorduncu M. Peridynamic differential operator for numerical analysis. New York, NY: Springer; 2019.
[45] Oterkus S, Madenci E, Agwai A. Peridynamic thermal diffusion. Journal of Computational Physics 2014;265:71–96.